

Real-time spectroscopy of transition states in bacteriorhodopsin during retinal isomerization

Takayoshi Kobayashi*, Takashi Saito* & Hiroyuki Ohtani†

* Department of Physics, Graduate School of Science, University of Tokyo, Hongo 7-3-1, Bunkyo, Tokyo 113-0033, Japan

† Department of Biomolecular Engineering, Graduate School of Bioscience and Biotechnology, Tokyo Institute of Technology, 4259, Nagatsuta, Yokohama 226-8501, Japan

Real-time investigations of the rearrangement of bonds during chemical transformations require femtosecond temporal resolution, so that the atomic vibrations within the reacting molecules can be observed. Following the development of lasers capable of emitting ultrashort laser flashes on this timescale, chemical reactions involving relatively simple molecules have been monitored in detail, revealing the transient existence of intermediate species as reactants are transformed into products^{1–3}. Here we report the direct observation of nuclear motion in a complex biological system, the retinal chromophore of bacteriorhodopsin (bR₅₆₈)⁴, as it undergoes the *trans*–*cis* photoisomerization that is fundamental to the vision process. By using visible-light pulses of less than 5 femtosecond in duration^{5,6}, we are able to monitor changes in the vibrational spectra of the transition state and thus show that despite photoexcitation of the anti-bonding molecular orbital involved, isomerization does not occur instantly, but involves transient formation of a so-called ‘tumbling state’. Our observations thus agree with growing experimental^{7–14} and *ab initio* evidence^{15,16} for a three-state photoisomerization

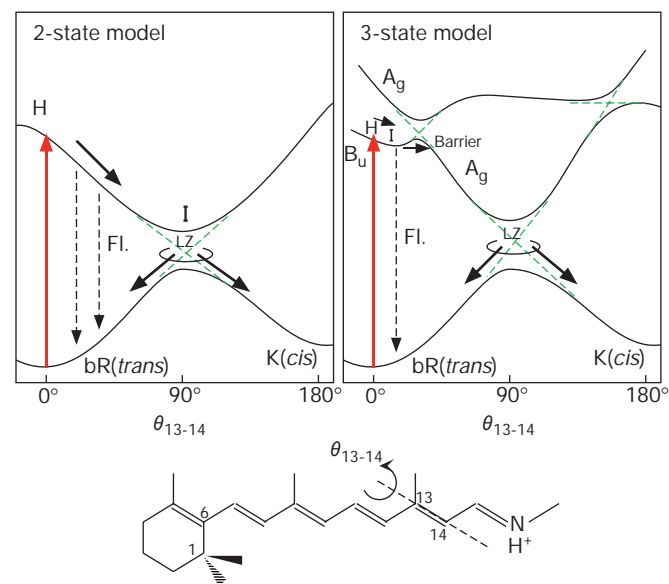


Figure 1 Schematic potential energy curves of two-state and three-state models along the torsional angle of the C₁₃ = C₁₄ bond of the protonated retinal Schiff base of bR₅₆₈. In the two-state model, the wave packet ‘slides down’ the barrier-free smooth potential surface along the C₁₃ = C₁₄ torsion coordinate from the Franck–Condon (H) state to the 90° rotated conformer (I) within 200 fs, and a temporal change in the emission spectrum (dynamic Stokes shift) is expected corresponding to the H → I₄₆₀ process. In the three-state model, the skeletally deformed state (I) is converted to a tumbling state with a time constant of 200 fs and then the torsional angle distribution becomes narrow. In both models K is in a cisoid conformation.

model^{8–10,17} and firmly discount the initially suggested two-state model^{18–20} for this process.

Using pulses shorter than 5 fs, we have succeeded in reaching the fundamental limit in resolving nuclear motion in a complex biological system. bR₅₆₈ undergoes the following photochemical cycle:



Here, H denotes the Franck–Condon excited state of bR₅₆₈ with an all-*trans* retinal Schiff base. The subscripts represent the wavelengths (in nm) of absorption maxima of the species. Several vibrational spectroscopy studies using ultrashort pulses^{7,21–24} have shown that H and I₄₆₀ are excited-state species with a chromophore of an all-*trans* conformation, and that K₆₁₀ is a ground-state species with the chromophore already converted to the 13-*cis* conformation. But the primary molecular processes between the H and K₆₁₀ states have been controversial, with two models discussed for the photoisomerization process: the two-state^{18–20} model and the three-state model^{8–10,17} (Fig. 1). However, recent experiments^{7–14} and *ab initio* calculations^{15,16} favour the three-state model, with changes in the molecule’s structure assumed to precede the *trans*–*cis* isomerization^{8–16}.

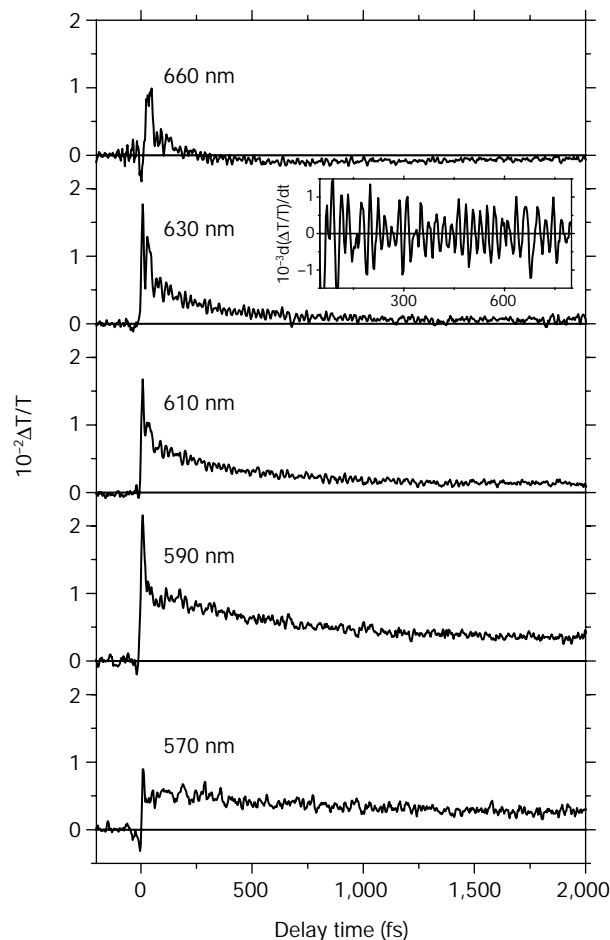


Figure 2 Time-dependence of the transmittance change ($\Delta T/T$) following sub-5-fs pulse excitation of a suspension of the light-adapted purple membrane of *Halobacterium salinarum* containing bR₅₆₈ at room temperature. Sub-5-fs pump and probe pulses (520–750 nm) were generated by non-collinear optical parametric amplification^{5,6}. The positive $\Delta T/T$ observed at wavelengths shorter than 630 nm is due to the bleaching of bR₅₆₈. At wavelengths longer than 660 nm, a negative signal due to the absorption of I (S_n–S₁ transition) appeared at 250 fs. The inset shows an enlarged trace monitored at 630 nm.

In order to elucidate the isomerization process in more detail, we measured the time-resolved transmittance change ($\Delta T/T$), which we call the real-time signal, of bR_{568} using sub-5-fs pulses as both pump and probe at room temperature. Figure 2 shows the real-time signals of bR_{568} at several wavelengths. The measured $\Delta T/T$ is modulated by molecular vibrations, which correspond to Raman-active modes^{25,26}. The Fourier transformation of $\Delta T/T$ around an arbitrary delay time t_d gives the amplitudes and frequencies of the molecular vibrations at t_d . Figure 3 shows spectrograms calculated for real-time signals probed at 610 nm. As shown in the spectrograms, instantaneous frequencies are modulated at a period of about 200 fs. This can be seen from the time-integrated Fourier power spectrum of the vibrationally induced transmittance modulation. Figure 4 shows the results of peak detection using the previously measured Raman frequencies^{23,27,28} for the 630-nm probe data. We conclude that the temporal shifts in frequency are due to wave-packet motion of the excited state rather than the ground state for the following reasons. (1) The spectrogram calculated for the real-time signal at 660 nm due to excited-state absorption (shown in Fig. 2) has the same features as those at other wavelengths. (2) The pulse width (sub-5-fs) is much shorter than the observed molecular vibration periods, and is too short to enhance the molecular vibration in the ground electronic state^{25,26}. (3) The decay of the molecular vibration amplitude is not longer than that of $\Delta T/T$.

The key feature of the spectrogram is the frequency of the ethylene-like symmetric C=C stretching modes in the 1,500–1,550 cm^{-1} region reflecting π -bond order. Interestingly, the peak frequency is modulated between 1,500 and 1,550 cm^{-1} . A similar

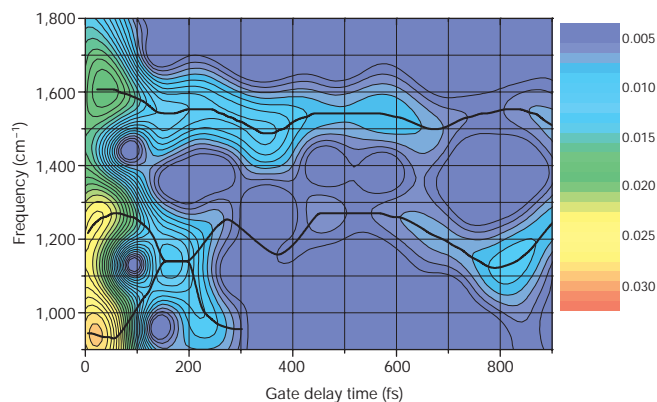


Figure 3 Spectrogram calculated for the trace at 610 nm. The calculations used the Hanning window function $W(t - t_d) = 1/2 + (1/2)\cos[\pi(t - t_d)/2\Delta t]$ with a 75-fs half-width at half-maximum (HWHM) of Δt and a peak at t_d (window delay time). The Fourier transformation of $\Delta T/T$ kinetics gives frequency information that corresponds to Raman frequency. The Fourier amplitude increases from blue to red (false colours). Black lines show the peaks of several modes strongly coupled to photoexcitation. The spectrogram shows the appearance of all the significant vibrations^{23,27,28} in the characteristic frequency ranges 1,500–1,650 cm^{-1} (C=C and C=N stretching modes), 1,150–1,250 cm^{-1} (in-plane C=C–H bending coupling with the C=C stretching modes) and 900–1,000 cm^{-1} (the hydrogen-out-of plane (HOOP) mode). The HOOP mode is inactive when the molecular structure is highly planar, and is enhanced by distortion of the molecular plane. The increase in the HOOP signal intensity just after excitation (30 fs) shows the distortion. The changes in the frequencies and amplitudes of HOOP and C=C–H in-plane-wagging can be seen following the progress of the twisting around the $\text{C}_{13}=\text{C}_{14}$ bond. Their frequencies cannot be discriminated at 150–200 fs because the in-plane and out-of-plane modes cannot be well defined owing to the non-planarity of the molecule. After that, these vibrations recover and then their intensities are reduced substantially because of the broad distributions of frequencies for the 200–600 fs region. The intensities partially recover when the frequency distributions become narrow owing to thermalization in the 700–900 fs region. This shows that isomerization from transoid to cisoid conformation followed by thermalization is over at this time region.

modulation of instantaneous frequencies has been observed for polydiacetylene (PDA) in previous work using the same sub-5-fs visible pulses^{29,30}. In PDA, the frequencies of C=C and C–C stretching are modulated at the vibrational period of the C=C–C bending mode (145 fs) for about 2 ps. The modulation frequency in bR_{568} was calculated to be 160 cm^{-1} from the Fourier transform calculation of the Fourier power spectrum, which corresponds to the 200-fs oscillation period of twisting around the C=C bond. To our knowledge, this is the first real-time observation of the frequency modulation of C=C stretching associated with the torsional motion relevant to the *trans*–*cis* isomerization. The frequency modulation induces the generation of side bands, but conventional Raman spectroscopy cannot discriminate the bands from modes existing accidentally nearby.

We now examine the contribution of the 200-fs torsional motion to the coupling of other vibrational modes by describing four events that occur on different timescales. The first event occurs within 50–100 fs. The wave-packet reaches the flat potential region (I_{460} with a B_u -like electronic configuration) from H. Periodic out-of-plane distortion also begins. An intense C=N stretching band from the protonated Schiff base ($\text{C}_{15}=\text{NH}^+$, 1,620–1,630 cm^{-1}) appears within 50 fs. Both the intensity and frequency of the band dramatically decrease within 100 fs. The fast dumping causes spectral broadening; although conventional methods cannot distinguish the homogeneous and inhomogeneous broadening, the method we describe here—of observing the time-dependent molecular vibration—can distinguish the two, by detecting the recurrence in the

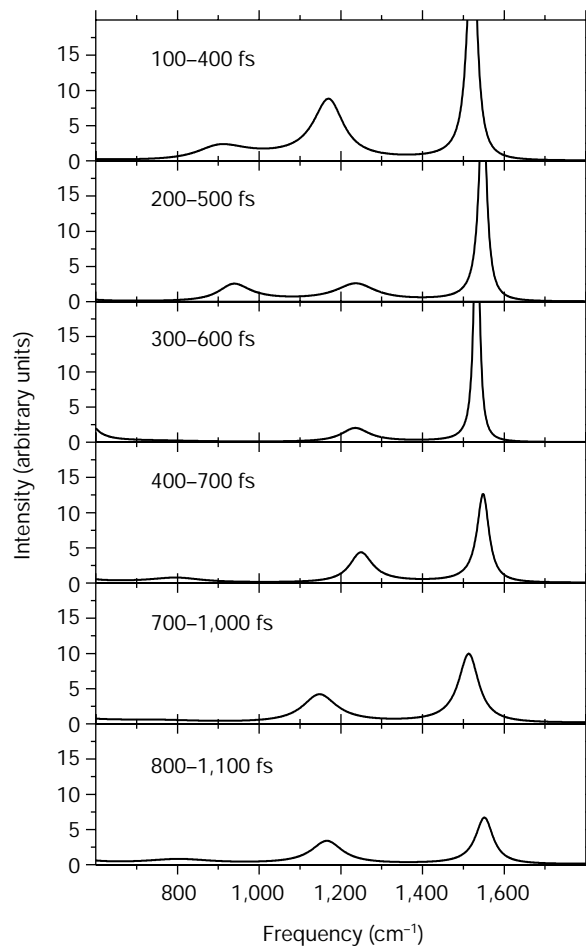


Figure 4 Fourier power spectrum of instantaneous frequencies appearing in the trace of transmittance change probed at 630 nm. The spectra were obtained by the maximum entropy method for the 300-fs rectangular gated signals.

case of inhomogeneous broadening. The fast frequency lowering indicates the effect of the torsional motion. The in-plane C=C-H bending modes coupled with C-C stretching modes appear in the 1,150–1,300 cm⁻¹ region, which is called the fingerprint region, because it is very sensitive to the chromophore conformation. The skeletal vibrations around 1,250 cm⁻¹ are activated in the first 100 fs as predicted theoretically^{15,16}. The hydrogen-out-of-plane (HOOP) modes appear just after the excitation in the 800–1,050 cm⁻¹ region. The intensity of the HOOP modes is sensitive to the tilting angle around the C=C bond. We expect that the HOOP intensity at first increases with the torsional angle, and then decreases or even disappears as the angle approaches 90°.

The second event is seen in the 100–200 fs region, and involves splitting of the band centred around 1,250 cm⁻¹ into two peaks about 100 fs after excitation of the chromophore. The frequency of one peak gradually increases, reaching 1,520–1,540 cm⁻¹ at about 150 fs, while the frequency of the other peak gradually decreases, reaching a value as low as 1,140 cm⁻¹ at 170 fs after excitation. The temporal shift of the frequency of the latter mode (C=C-H in-plane bending) is correlated with that of the HOOP band. These frequencies are modulated with the 200-fs period of the C=C torsion. The peak positions of the HOOP mode and the in-plane C=C-H bending modes are well separated in the region below 100 fs, but not in the 150–200 fs region. These mode frequencies approach each other and merge into a single peak, as there is neither an in-plane nor an out-of-plane mode in a distorted configuration. The two modes reappear in the region slightly longer than 250 fs, where planarity is recovered. This suggests that the *trans*→13-*cis* isomerization occurred within less than 200 fs according to the two-state model. However, the product K₆₁₀ has not yet been formed. For the *t_d* > 200 fs region, the intensities of the C=C-H bending and HOOP modes become very weak at all the probe photon energies studied (610–680 nm, data not shown). Therefore, the coincident increase and decrease of the frequencies of the HOOP and in-plane C=C-H bending modes strongly indicate that the torsional

motion modifies the frequencies of both the out-of-plane and in-plane bending-mode frequencies with a period of 200 fs.

The third event is the formation of the transition state in the 200–600 fs region. C=N stretching, C=C-H bending, and HOOP modes are also silent in this region. The weak intensity is partly due to the broad distribution of molecular conformations covered by the wave packet. Energy randomization occurs during the fast wave-packet motion along the potential curves of the excited B_u-like and A_g-like states, and during the Landau-Zener (LZ) tunnelling in between B_u and A_g. However, the isomerization in the C₁₃=C₁₄ bond has not occurred at this stage. The skeletal change precedes the isomerization. We call the molecular state in the 200–600 fs region a ‘tumbling state’. In this state, the intensity reduction of C=C stretching is not as drastic as those of the HOOP and in-plane bending, as the number of the C=C stretching modes is larger than that of the C=C-H configuration, and the C=C stretching is less sensitive to the torsional angle than the HOOP and in-plane bending modes. These features can be explained by the torsional motion of the two moieties of the retinal Schiff base separated by the C₁₃=C₁₄ double bond just after excitation, as shown in Fig. 5. The torsional motion and the broadening due to the inhomogeneity of the torsional angles and the rapid change in frequencies induce the reduction of the intensities of the corresponding vibrational bands.

The final event occurs 700 fs later. At 700–900 fs, the intensities of the in-plane C=C-H bending and C=C stretching modes (1,150–1,250 cm⁻¹) are partially recovered, owing to the narrowing of the torsional angle distribution in the quasi-thermal state after relaxing to the bottom of the potential curve of the A_g-like excited state along the torsional angle coordinate. After this relaxation to the ground state, the conformational change takes place again through LZ tunnelling to the 13-*cis* conformation, that is, K₆₁₀, with 55% efficiency¹⁴. This verifies that the oscillating signal is not caused by the molecular vibration in the ground electronic state, but by vibration in the excited states. The gate delay time of 700–800 fs corresponds to the period of the population thermalized before it is converted to the K intermediate. □

Received 14 May; accepted 21 September 2001.

- Polanyi, J. C. & Zewail, A. H. Direct observation of the transition state. *Acc. Chem. Res.* **28**, 119–132 (1995).
- Rose, T. S., Rosker, M. J. & Zewail, A. H. Femtosecond real-time observation of wave packet oscillations (resonance) in dissociation reactions. *J. Chem. Phys.* **88**, 6672–6673 (1988).
- Rose, T. S., Rosker, M. J. & Zewail, A. H. Femtosecond real-time probing of reactions. IV. The reactions of alkali halides. *J. Chem. Phys.* **91**, 7415–7436 (1989).
- Oesterheld, D. & Stoekenius, W. in *Methods of Enzymology, Biomembranes Part A*, Vol. 31 (eds Freischer, S. and Packer, L.) 667–678 (Academic, New York, 1974).
- Shirakawa, A., Sakane, I. & Kobayashi, T. Pulse-front-matched optical parametric amplification for sub-10-fs pulse generation tunable in the visible and near infrared. *Opt. Lett.* **23**, 1292–1294 (1998).
- Shirakawa, A., Sakane, I., Takasaka, M. & Kobayashi, T. Sub-5-fs visible pulse generation by pulse-front-matched noncollinear optical parametric amplification. *Appl. Phys. Lett.* **74**, 2268–2270 (1999).
- Atkinson, G. H., Uji, L. & Zhou, Y. Vibrational spectrum of the J-625 intermediate in the room temperature bacteriorhodopsin photocycle. *J. Phys. Chem. A* **104**, 4130–4139 (2000).
- Hasson, K. C., Gai, F. & Anfinsen, P. A. The photoisomerization of retinal in bacteriorhodopsin: experimental evidence for a three-state model. *Proc. Natl Acad. Sci. USA* **93**, 15124–15129 (1996).
- Haran, G. *et al.* Excited state dynamics of bacteriorhodopsin revealed by transient stimulated emission spectra. *Chem. Phys. Lett.* **261**, 389–395 (1996).
- Gai, F., Hasson, K. C., McDonald, J. C. & Anfinsen, P. A. Chemical dynamics in proteins: the photoisomerization of retinal in bacteriorhodopsin. *Science* **279**, 1886–1891 (1998).
- Humphrey, W., Lu, H., Logonov, I., Werner, H.-J. & Schulten, K. Three electronic state model of the primary phototransformation of bacteriorhodopsin. *Biophys. J.* **75**, 1689–1699 (1998).
- Zhong, Q., Ruhman, S. & Ottolenghi, M. Reexamining the primary light-induced events in bacteriorhodopsin using a synthetic C13=C14-locked chromophore. *J. Am. Chem. Soc.* **118**, 12828–12829 (1996).
- Ye, T. *et al.* On the nature of the primary light-induced events in bacteriorhodopsin: ultrafast spectroscopy of native and C13=C14 locked pigments. *J. Phys. Chem. B* **103**, 5122–5130 (1999).
- Song, L. & El-Sayed, M. A. Primary step in bacteriorhodopsin photosynthesis: bond stretch rather than angle twist of its retinal excited-state structure. *J. Am. Chem. Soc.* **120**, 8889–8890 (1998).
- Vreven, T. *et al.* Ab initio photoisomerization dynamics of a simple retinal chromophore model. *J. Am. Chem. Soc.* **119**, 12687–12688 (1997).
- Garavelli, M., Negri, F. & Olivucci, M. Initial excited-state relaxation of the isolated 11-*cis* protonated Schiff base of retinal: Evidence for in-plane motion from ab initio quantum chemical simulation of the resonance Raman spectrum. *J. Am. Chem. Soc.* **121**, 1023–1029 (1999).
- Du, M. & Fleming, G. R. Femtosecond time resolved fluorescence spectroscopy of bacteriorhodopsin: direct observation of excited state dynamics in the primary step of the proton pump cycle. *Biophys. Chem.* **48**, 101–111 (1993).

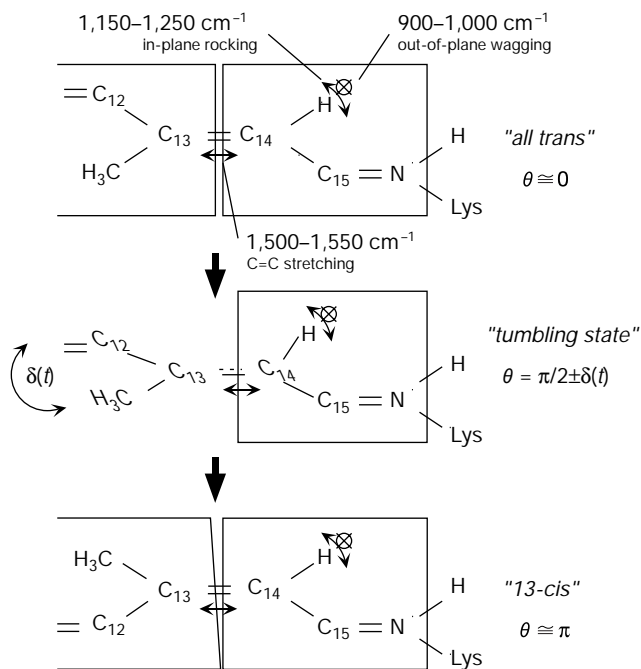


Figure 5 A mechanism of the *trans*–*cis* photoisomerization of the retinal chromophore. After photoexcitation of bR₅₆₈ to the Franck–Condon state (H), two moieties are rotated with respect to each other to a skeletally deformed state (K₄₆₀; top) and then to a tumbling state (middle) and then to a *cis* conformation (K₆₁₀; bottom).

18. Peteanu, L. A., Shoenlein, R. W., Wang, Q., Mathies, R. A. & Shank, C. V. The first step in vision occurs in femtoseconds: complete blue and red spectral studies. *Proc. Natl Acad. Sci. USA* **90**, 11762–11766 (1993).

19. Shoenlein, R. W., Peteanu, L. A., Wang, Q., Mathies, R. A. & Shank, C. V. Femtosecond dynamics of cis-trans isomerization in a visual pigment analog: isorhodopsin. *J. Phys. Chem.* **97**, 12087–12092 (1993).

20. Mathies, R. A., Brito Cruz, C. H., Pollard, W. T. & Shank, C. V. Direct observation of the femtosecond excited-state cis-trans isomerization in bacteriorhodopsin. *Science* **240**, 777–779 (1988).

21. Atkinson, G. H., Brack, T. L., Blanchard, D. & Rumbles, G. Picosecond time-resolved resonance Raman spectroscopy of the initial trans to cis isomerization in the bacteriorhodopsin photocycle. *Chem. Phys.* **131**, 1–15 (1989).

22. van den Berg, R., Jang, D. J., Bitting, H. C. & El-Sayed, M. A. Subpicosecond resonance Raman spectra of the early intermediates in the photocycle of bacteriorhodopsin. *Biophys. J.* **58**, 135–141 (1990).

23. Doig, S. J., Reid, P. J. & Mathies, R. A. Picosecond time-resolved resonance Raman spectroscopy of bacteriorhodopsin J, K, and KL intermediates. *J. Phys. Chem.* **95**, 6372–6379 (1991).

24. Diller, R. *et al.* Femtosecond time-resolved infrared laser study of the J-K transition of bacteriorhodopsin. *Chem. Phys. Lett.* **241**, 109–115 (1995).

25. Pollard, W. T. *et al.* Theory of dynamic absorption spectroscopy of nonstationary states. 4. Application to 12-fs resonant impulsive Raman spectroscopy of bacteriorhodopsin. *J. Phys. Chem.* **96**, 6147–6158 (1992).

26. Bardeen, C. J., Wang, Q. & Shank, C. V. Femtosecond chirped pulse excitation of vibrational wave packets in LD690 and bacteriorhodopsin. *J. Phys. Chem. A* **102**, 2759–2766 (1998).

27. Eyring, G., Curry, B., Broek, A., Lugtenburg, J. & Mathies, R. Assignment and interpretation of hydrogen out-of-plane vibrations in the resonance Raman spectra of rhodopsin and bathorhodopsin. *Biochemistry* **21**, 384–393 (1982).

28. Myers, A. B., Harris, R. A. & Mathies, R. A. Resonance Raman excitation profiles of bacteriorhodopsin. *J. Chem. Phys.* **79**, 603–613 (1983).

29. Kobayashi, T., Shirakawa, A., Matsuzawa, H. & Nakanishi, H. Real-time vibrational mode-coupling associated with ultrafast geometrical relaxation in polydiacetylene induced by sub-5-fs pulses. *Chem. Phys. Lett.* **321**, 385–393 (2000).

30. Kobayashi, T. & Shirakawa, A. Tunable visible and near-infrared pulse generator in a 5 fs regime. *Appl. Phys. B* **70**, S239–S246 (2000).

Acknowledgements

We thank J. Watson and M. Murao for careful reading of the manuscript. This work was partially supported by the Research for the Future program run by the Japan Society for Promotion of Science (T.K.), the Special Coordination Funds (“Molecular Sensors for Aero-Thermodynamic Research”; H.O.) and Scientific Research (H.O.) of the Ministry of Education, Culture, Sports, Science and Technology.

Correspondence and requests for materials should be addressed to T.K. (e-mail: kobayashi@phys.s.u-tokyo.ac.jp).

Systematic distortions in world fisheries catch trends

Reg Watson* & Daniel Pauly*

* Fisheries Centre, 2204 Main Mall, University of British Columbia, Vancouver, British Columbia V6T 1Z4, Canada

Over 75% of the world marine fisheries catch (over 80 million tonnes per year) is sold on international markets, in contrast to other food commodities (such as rice)^{1,2}. At present, only one institution, the Food and Agriculture Organization of the United Nations (FAO) maintains global fisheries statistics. As an inter-governmental organization, however, FAO must generally rely on the statistics provided by member countries, even if it is doubtful that these correspond to reality. Here we show that misreporting by countries with large fisheries, combined with the large and widely fluctuating catch of species such as the Peruvian anchoveta, can cause globally spurious trends. Such trends influence unwise investment decisions by firms in the fishing sector and by banks, and prevent the effective global management of international fisheries.

World fisheries catches have greatly increased since 1950, when the FAO of the United Nations began reporting global figures³. The reported catch increases were greatest in the 1960s, when the traditional fishing grounds of the North Atlantic and North Pacific became fully exploited, and new fisheries opened at lower latitudes

and in the Southern Hemisphere. Global catches increased more slowly after the 1972 collapse of the Peruvian anchoveta fishery⁴, the first fishery collapse that had repercussions on global supply and prices of fishmeal (Fig. 1a). Even taking into account the variability of the anchoveta, global catches were therefore widely expected to plateau in the 1990s at values of around 80 million tonnes, especially as this figure, combined with estimated discards of 16–40 million tonnes⁵, matched the global potential estimates published since the 1960s (ref. 6). Yet the global catches reported by the FAO generally increased through the 1990s, driven largely by catch reports from China.

These reports appear suspicious for the following three reasons: (1) The major fish populations along the Chinese coast for which assessments were available had been classified as overexploited decades ago, and fishing effort has since continued to climb^{7,8}; (2) Estimates of catch per unit of effort based on official catch and effort statistics were constant in the Yellow, east China and south China seas from 1980 to 1995 (ref. 9), that is, during a period of continually increasing fishing effort and reported catches, and in contrast to declining abundance estimates based on survey data⁷; (3) Re-expressing the officially reported catches from Chinese waters on

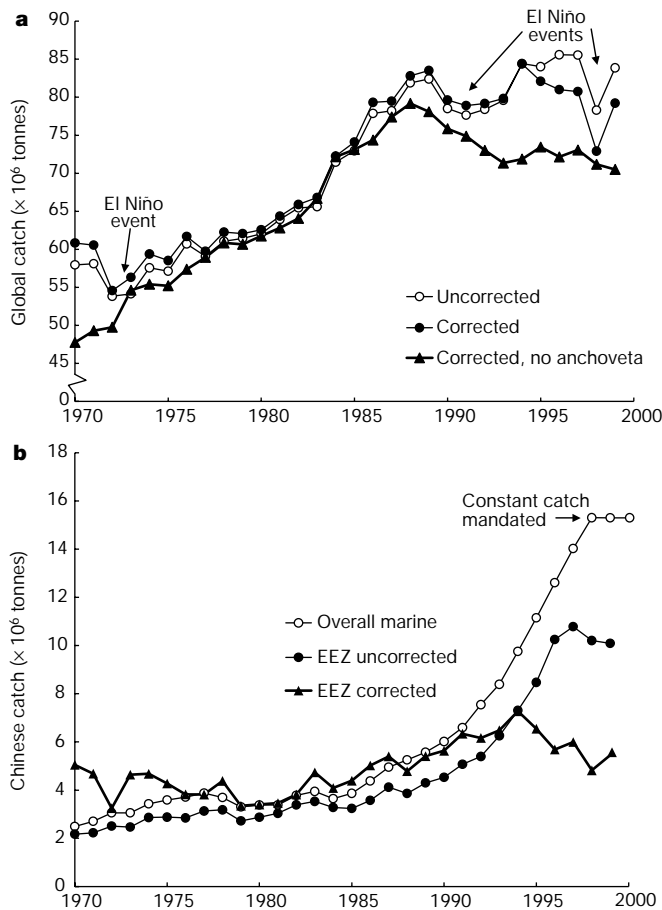


Figure 1 Time series of global and Chinese marine fisheries catches (1950 to present). **a**, Global reported catch, with and without the highly variable Peruvian anchoveta. Uncorrected figures are from FAO (ref. 3); corrected values were obtained by replacing FAO figures by estimates from **b**. The response to the 1982–83 El Niño/Southern Oscillation (ENSO) is not visible as anchoveta biomass levels, and hence catches were still very low from the effect of the previous ENSO in 1972 (ref. 4). **b**, Reported Chinese catches (from China’s exclusive economic zone (EEZ) and distant water fisheries) increased exponentially from the mid-1980s to 1998, when the ‘zero-growth policy’ was introduced. The corrected values for the Chinese EEZ were estimated from the general linear model described in the Methods section.